

Joint Camera Intrinsic and LiDAR-Camera Extrinsic Calibration

Guohang Yan, Feiyu He, Chunlei Shi, Xinyu Cai and Yikang Li[†]

Abstract—Sensor-based environmental perception is a crucial step for autonomous driving systems, for which an accurate calibration between multiple sensors plays a critical role. For the calibration of LiDAR and camera, the existing method is generally to calibrate the intrinsic of the camera first and then calibrate the extrinsic of the LiDAR and camera. If the camera’s intrinsic is not calibrated correctly in the first stage, it isn’t easy to calibrate the LiDAR-camera extrinsic accurately. Due to the complex internal structure of the camera and the lack of an effective quantitative evaluation method for the camera’s intrinsic calibration, in the actual calibration, the accuracy of extrinsic parameter calibration is often reduced due to the tiny error of the camera’s intrinsic parameters. To this end, we propose a novel target-based joint calibration method of the camera intrinsic and LiDAR-camera extrinsic parameters. Firstly, we design a novel calibration board pattern, adding four circular holes around the checkerboard for locating the LiDAR pose. Subsequently, a cost function defined under the reprojection constraints of the checkerboard and circular holes features is designed to solve the camera’s intrinsic parameters, distortion factor, and LiDAR-camera extrinsic parameter. In the end, quantitative and qualitative experiments are conducted in actual and simulated environments, and the result shows the proposed method can achieve accuracy and robustness performance. The open-source code is available at <https://github.com/OpenCalib/JointCalib>.

I. INTRODUCTION

Autonomous driving has attracted more and more attention in both industry and academic fields. A safe and robust driving relies on an accurate sensor-based environmental perception system. However, a single sensor can not guarantee reliability because of the diverse conditions in the real world. To ensure that autonomous driving vehicles can operate appropriately under dynamic circumstances, multi-model complementary sensors cooperation technologies have appeared, which can provide adequate environmental information, thus contributing to a more reliable data fusion. Among the numerous types of sensor data fusion methods, the combination of LiDAR and camera is one of the most commonly used pairs of sensors for driving environment perception. LiDARs can provide 3D point cloud data, which include accurate depth and reflection intensity information, while cameras capture the rich semantic information of the scene. The combination of camera and LiDAR provides the feasibility to overcome the flaws of each sensor. The main challenge in fusing these two heterogeneous sensors is to find the precise camera’s intrinsic parameters and the rigid

body transformation between sensor coordinate systems by performing extrinsic calibration [1]. Researchers have made a lot of effort to improve the accuracy and efficiency of calibration results, such as specific targets like checkerboards [2]–[6], spherical target [7], gray code [8], multi-plane stereo target [9] and semantic objects [10].

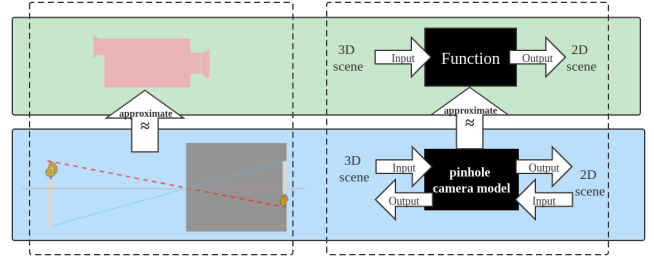


Fig. 1: The process of calibrating the camera’s intrinsic parameters through a pinhole model.

However, existing calibration methods suffer from various problems. The first issue is the reliability of the camera’s intrinsic parameters because most methods assume the camera’s intrinsic parameters are known or compute them through Zhang’s process [11]. The pinhole model is usually used when calibrating the camera’s intrinsic, but the actual camera projection process and the pinhole model are not completely corresponding [12]. The actual camera lens group is more complex and does not have an absolute optical center point [13]. As shown in Fig. 1, the whole calibration process is an approximation measure. At the same time, due to the defects of the camera structure and the uncertainty in the optimization of nonlinear functions, the obtained solution is usually suboptimal. Consequently, the accuracy of extrinsic calibration will be affected. Our experiment of the camera’s intrinsic calibration consistency also demonstrates the camera’s intrinsic calibration volatility.

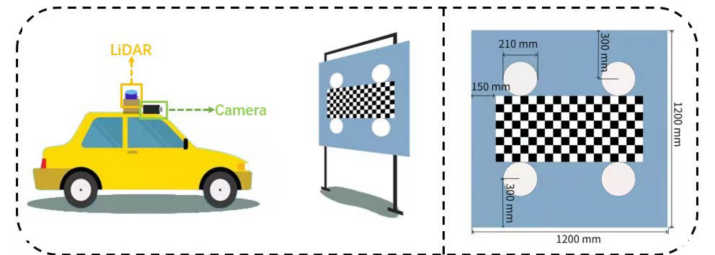


Fig. 2: A novel calibration board pattern.

In this paper, we present a novel joint calibration method that overcomes the inaccurate extrinsic calibration of LiDAR

[†] Corresponding author.

Guohang Yan, Feiyu He, Chunlei Shi, Xinyu Cai and Yikang Li are with Autonomous Driving Group, Shanghai AI Laboratory, China. {yanguohang, hefeiyu, zhangchunlei, caixinyu, liyikang}@pjlab.org.cn

and camera caused by imperfect camera intrinsic parameters. Unlike existing calibration methods that only estimate the rotation and transformation between two sensor frames, the output of the proposed method contains the camera's intrinsic parameters, distortion factor, and LiDAR-camera extrinsic parameters.

Firstly, as shown in Fig. 2, we design a novel calibration board pattern, which contains a checkerboard used for the calibration of the camera's intrinsic parameters and several circular holes for locating the LiDAR point cloud. We first calibrate the camera initial intrinsic and board-camera initial extrinsic parameter by Zhang's method [11]. Then, 2D circles center points on the image are calculated from these parameters and the calibration board size. By extracting the position of the circles center in LiDAR, we can project the circles center 3D points to the image plane by the LiDAR-camera calibration parameters. The calculated 2D points and the projected 2D points form multiple 2D point pairs. We use the Euclidean distance between these point pairs to refine the calibration parameters. At the same time, the constraints on reprojection of 3D-2D points of checkerboard corners are added to the optimization process.

The contributions of this work is listed as follows:

- 1) We design a novel calibration board pattern and propose a target-based joint calibration method of the camera intrinsic and LiDAR-camera extrinsic parameters.
- 2) The calibration of the LiDAR-camera is formulated as a nonlinear optimization function by minimizing the reprojection error between the 3D-2D point pairs of circles center and checkerboard corners on the calibration board.
- 3) We develop a practical calibration software and open source it on GitHub to benefit the community.

II. RELATED WORK

Researchers have proposed many approaches to address the intrinsic and extrinsic calibration of multi-model sensor calibration. Intrinsic calibration estimates the operational parameters of sensors and is usually performed before performing the extrinsic calibration. Typically, camera intrinsic calibration focus on estimating focal length, distortion factor, and skewness. Escalera et al. [14] find both camera's intrinsic and extrinsic parameters by detecting corner points and extracting horizontal and vertical sets of lines from a checkerboard. Bogdan et al. [15] estimate the focal length and distortion factor by a learning-based approach, and three different network architectures are proposed. Jin et al. [16] calibrate the intrinsic parameters of depth camera with cuboids, then optimize an objective function based on the distance error and angle error from reference cuboids. An et al. [17] apply Charuco board to overcome the defects of checkerboard and ArUco board by building a Charuco board-based cube structure for feature points extraction, which can be used to estimate perspective projection matrix and solve the intrinsic parameters. Lopez et al. [18] predict the extrinsic and intrinsic camera parameters through a single

image by training a convolutional neural network. Instead of predicting the intrinsic parameters directly, they use proxy variables such as distorted offset to increase the visibility of the training process.

By contrast, extrinsic calibration estimates the rigid body transform between different sensor frames [19]. According to the requirement of auxiliary equipment, extrinsic calibration can be divided into two categories: target-based and target-less procedures.

A. Target-based Method

Target-based extrinsic calibration methods are widely used in the sensors calibration procedure. Researchers have designed various kinds of calibration targets to meet the characteristics of different sensors. Zhang et al. [20] solve the extrinsic parameters based on a checkerboard and refine them by minimizing the re-projection error of laser points to the checkerboard plane. The method is easy to implement but cannot obtain the optimal solution directly. Geiger et al. [21] propose an approach to calibrate LiDAR to the camera by extracting the corner points from both point cloud and image, then estimate the rotation and translation by maximizing the alignments of normal vectors and minimizing point-to-plane distances respectively. Finally, the fine registration is performed based on gradient descent. Huang et al. [22] perform extrinsic calibration by extracting vertices of the target from point cloud and image plane, and optimize the result by formulating a Perspective-n-Points problem which minimizes Euclidean distance of the corresponding corners. Intersection over Union (IoU) is also used for further refinement. Zhou et al. [23] find the extrinsic parameters by computing the correspondences of line features in both LiDAR and camera frame, and refine the initial solution through a nonlinear optimization problem.

B. Target-less Method

Target-less method usually takes advantage of natural environmental features (such as lines) from the scene, by solving the geometric constraints, the extrinsic parameters can be derived. Levinson et al. [24] propose an online extrinsic calibration method by measuring the edge alignment. Edges in LiDAR points and image are extracted by depth discontinuity and Inverse Distance Transform (IDT) respectively, then minimize the re-projection error of 3D LiDAR edge points to the edge image to obtain the optimal solution. Ma et al. [25] calibrate camera to range sensor extracting line features in road scene, through segmentation and line fitting, three 3D-2D line pairs that do not intersect at the same point are extracted and thus formulate a Perspective-3-Lines problem which provides the initial calibration, and refine it based on a random search algorithm on the 6-DoF parameters. Pandey et al. [26] use the reflection intensity measured by LIDAR and intensity values from camera and derive the optimal extrinsic parameters by maximizing a objective function based on mutual information. Similarly, Taylor et al. [27] perform LiDAR-camera calibration by normalizing the mutual information, and maximizing the gradient correlation of image

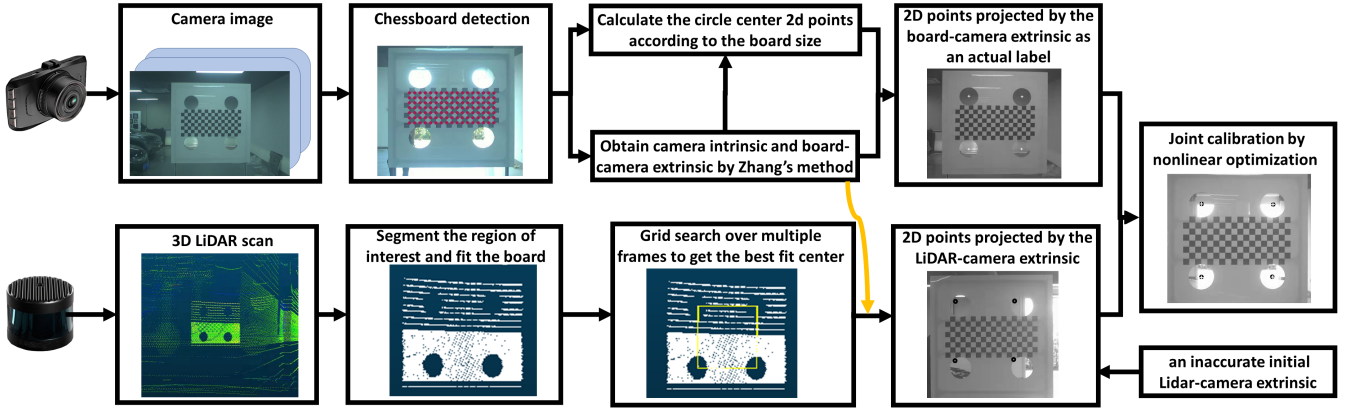


Fig. 3: Overview of the different stages of the presented method.

and LiDAR points. However, extracting useful features from natural scene is quite challenging, since the environment is usually unstructured and dynamic, which might cause the loss of precision. Target-based approach avoid this difficulty by using calibration targets to ensure the features can be extracted robustly and accurately. Nevertheless, both of the two methods solely solve the intrinsic parameters before extrinsic calibration. In contrast to the discussed related work, we provide a joint intrinsic and extrinsic calibration approach that output intrinsic and extrinsic parameters at the same time.

III. METHODOLOGY

This section introduces the details of our approach, including calibration target design, calibration target detection, calibration data collection, and calibration optimization process. Fig. 3 shows the overview of the presented method.

A. Calibration target design

A well-designed calibration target should satisfy the following properties (i) detectable in all relevant sensors and (ii) observable features extracted for localization. Based on the working principles of LiDAR and camera, depth discontinuous such as edges for point cloud and corners in the image is most widely used as calibration features since they can be detected accurately and robustly. As discussed in [28], circular-shaped targets are more robust to be detected than rectangular shapes because they can interact with several LiDAR scans horizontally and vertically without missing edge information. As shown in Fig. 2, our design of calibration target combined both geometrical and visual characteristics, which is suitable for keypoints detection in LiDAR and camera modalities. We put one black and white checkerboard in the center, surrounded by four circular holes. On the one hand, the holes can use geometrical discontinuities in LiDAR point clouds. On the other hand, the checkerboard corners can provide spatial constraints. Fig. 2 also shows the details of our calibration target with a specific size.

B. Calibration target detection

The first step of target-based calibration is to locate the spatial position of the calibration in each sensor frame. LiDAR sensor returns the 3D position while camera returns the colored 2D image of the target. Here we conduct the extraction procedures of checkerboard and circular holes separately. There are many existing techniques for detecting the checkerboard from the image, for example, using popular computer vision libraries. In this work, we choose OpenCV [29] library for checkerboard detection. As for LiDAR data, different from the method mentioned in [30], we locate each center of holes by generating a point cloud mask \mathcal{P}_{mask}^L , which has the same geometric structure as the calibration target.

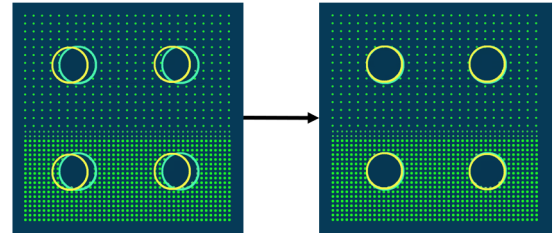


Fig. 4: The process of accurately extracting the center of the circle on the calibration board.

We assume the original point cloud data scanned by a LiDAR sensor is represented as \mathcal{P}_0^L . Firstly, in order to filter outliers and remove the noise of the surrounding environment, we segment the regions of interest by presetting detection range. Then the calibration target plane is segmented from \mathcal{P}_0^L through RANSAC plane fitting with orientation constraints, which is denoted by \mathcal{P}_{target}^L . Afterwards, we follow the grid search method described in [24] to find the best match of \mathcal{P}_{mask}^L and \mathcal{P}_{target}^L in LiDAR coordinate system $\{L\}$. Rather than searching on 6-DoF, here we focus on the yaw angle for rotation and x, y for translation relative to the calibration board. Fig. 4 illustrates the principle of the matching procedure, when perfect alignment achieved, least number of points will fall into the circular holes, and thus

the 3D position of each hole center can be located in $\{L\}$. Compared with [30], our method only requires the coordinate of the 3D point cloud without using additional intensity and ring id information, and the generated mask fixes the relative position between holes, which greatly improves the robustness and accuracy of center detection. Finally, each calibration board can obtain the center points of the four circular holes in the LiDAR coordinate system.

C. Calibration data collection

The calibration data collection process is similar to the camera's intrinsic calibration data collection. In order to ensure the calibration accuracy, checkerboard corner features and circular hole features need to be collected in each area of the image. In our experiment, both point clouds and images are collected in a stationary environment. As shown in Fig. 11, at least twenty frames of data need to be acquired for each calibration. In order to increase the density of LiDAR point clouds, ten frames of LiDAR point cloud are collected for each frame of the image.

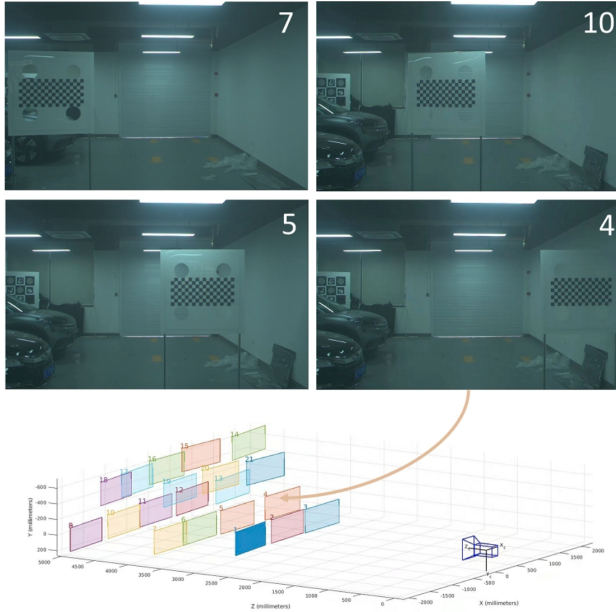


Fig. 5: Calibration data collection method

D. Calibration optimization process

1) *Circle Center 2D Points Calculation:* For the extracted LiDAR 3D circles center points, we need to get the corresponding 2D points on the image. We first calibrate the camera intrinsic \mathcal{K} , distortion factor and board-camera extrinsic $\mathbf{T}(t_x, t_y, t_z, r_x, r_y, r_z)$ by checkerboard corners. According to the size of the calibration board, we get the four circles center points $P_B = \{p_b^1, p_b^2, \dots, p_b^4\} \in \mathbb{R}^3$ of each calibration board, where B represents the coordinate system of the calibration board. The transformed point \mathbf{p}_c^i is then projected onto the camera image plane by \mathcal{K} and \mathbf{T} .

$$\mathbf{p}_c^i = \mathcal{K}(\mathbf{R}(\mathbf{r}) \cdot \mathbf{p}_b^i + \mathbf{t}), \quad k = 1, 2, \dots, 4. \quad (1)$$

where $\mathbf{R}(\mathbf{r})$ represents the rotation and can be parameterized by angle-axis representation \mathbf{r} . \mathbf{t} represents the translation with $\mathbf{t} = (t_x, t_y, t_z)^T$. After adding distortion factor, the actual location of the projected point $p_i = (u_i, v_i)$ is

$$\mathbf{p}_i = \mathbf{D}(\mathbf{p}_c^i), \quad (2)$$

$\mathbf{D}(p)$ is the camera distortion model. The extracted LiDAR 3D circles center points and the calculated 2d circles center points form multiple 3D-2D point pairs.

2) *Calibration optimization:* Through the previous process, multiple sets of 3D-2D point pairs of the circles center and the checkerboard corners on the calibration board are obtained. The 3D points $P_L \in \mathbb{R}^3$ of the circle center is in the LiDAR coordinate system $\{L\}$, and the 3D points $P_B \in \mathbb{R}^3$ of the chessboard corner is in the coordinate system $\{B\}$ of the calibration board. 2D points are pixels $P_C \in \mathbb{R}^2$ on the image. The optimization process aims to find the optimal LiDAR-camera extrinsic, camera's intrinsic and the distortion factor that minimizes the reprojection error between 3D-2D point pairs when projecting 3D points to 2D images. The process of projecting 3D points onto the image is as follows:

$$\frac{1}{Z_C} \begin{bmatrix} x \\ y \\ 1 \end{bmatrix} = \begin{bmatrix} f_x & 0 & c_x \\ 0 & f_y & c_y \\ 0 & 0 & 1 \end{bmatrix} \begin{bmatrix} r_{11} & r_{12} & r_{13} & t_1 \\ r_{21} & r_{22} & r_{23} & t_2 \\ r_{31} & r_{32} & r_{33} & t_3 \end{bmatrix} \begin{bmatrix} X \\ Y \\ Z \\ 1 \end{bmatrix} \quad (3)$$

where $\mathbf{p} = (X, Y, Z)^T \in \mathbb{R}^3$ represents LiDAR coordinate 3D point or calibration board coordinate 3D point, Z_C represents the Z coordinate in the camera coordinate system. The parameters to be optimized are $\mathbf{R} = \{r_{11}, r_{12}, \dots, r_{33}\}$ represents the rotation matrix, $\mathbf{t} = \{t_1, t_2, t_3\}$ represents the translation, and $\mathbf{K} = \{f_x, f_y, c_x, c_y\}$ represents the camera's intrinsic. The distortion model of the camera is as follows:

$$\begin{aligned} r^2 &= x * x + y * y, \quad r^4 = r^2 * r^2, \quad r^6 = r^4 * r^2 \\ u &= x(1 + k_1 r^2 + k_2 r^4 + k_3 r^6) + 2p_1 xy + p_2(r^2 + 2x^2) \\ v &= y(1 + k_1 r^2 + k_2 r^4 + k_3 r^6) + p_1(r^2 + 2y^2) + 2p_2 xy \end{aligned} \quad (4)$$

where $\mathbf{D} = \{k_1, k_2, p_1, p_2, k_3\}$ represents the distortion factor, $p = (u, v)$ represents the projection point on the image.

Next, we get the optimization equation based on the circles center and the checkerboard corners through the above projection process. The checkerboard corners reprojection error of the calibration board is

$$\mathcal{J}_{board} = \sum_{(u,v) \in P_B} (||u - u_{det}||_2 + ||v - v_{det}||_2) \quad (5)$$

where (u, v) represents the pixel coordinate point of the P_B projection, (u_{det}, v_{det}) is the actual detected pixel point. Here are the extrinsic parameters from the calibration board to the camera. The circles center reprojection error of the calibration board is

$$\mathcal{J}_{lidar} = \sum_{(u,v) \in P_L} (||u - u_{det}||_2 + ||v - v_{det}||_2) \quad (6)$$

where (u, v) represents the pixel coordinate point of the P_L projection, (u_{det}, v_{det}) is the actual calculated pixel point.

Here are the extrinsic parameters from the LiDAR to the camera.

The whole calibration process aims to achieve better alignment between LiDAR point cloud and image with satisfying the checkerboard corner constraints, which is also considered one of the critical evaluation criteria. The number of checkerboard corners on our calibration board is much more than the number of circular holes. Therefore, the weight of LiDAR-camera alignment error is greater than that of board-camera alignment error to balance the effects of two-loss functions. In sum, we minimize the following objective function:

$$\mathcal{J}_{sum} = \alpha \mathcal{J}_{board} + \beta \mathcal{J}_{lidar} \quad (7)$$

In our experiment, α is set to 1, and β is set to 60.

3) *Nonlinear Solution*: The rotation matrix uses nine vectors to describe the rotation of 3 degrees of freedom, which is redundancy. Furthermore, the rotation matrix has to be an orthogonal matrix with determinant 1. These constraints increase the difficulty of the solution when estimating or optimizing rotation matrices. A better way to represent the rotation matrix is using the angle-axis rotation vector. In our implementation, an inaccurate initial Lidar-camera extrinsic are provided as initialization, and the calibration optimization equation is solved by the Ceres solver [31].

IV. EXPERIMENTS

The experiment in this paper consists of two parts: a realistic experiment on our driverless vehicle test platform and a simulated experiment based on the Carla engine [32]. The results show that the proposed method is superior to the state-of-the-art in terms of accuracy and robustness.

A. Realistic Experiment

We conducted experiments on real driverless platforms, Fig. 6 shows our realistic experiment setup.

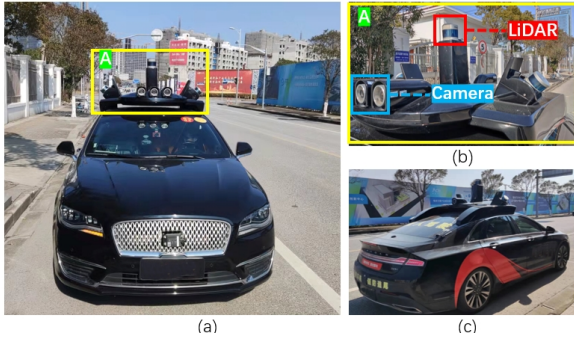


Fig. 6: Our sensor suit. Top is Hesai Pandar64 LiDAR. Front is the camera Balser acA1920-40gc with different FOVs ($FOV = 30^\circ$, $FOV = 60^\circ$, $FOV = 120^\circ$).

1) *Camera Intrinsic Calibration Consistency Evaluation*: Due to the complex internal structure of the camera and the way of data acquisition, the camera's intrinsic parameters are usually unstable in calibration [12]. On the other hand, the inaccuracy of the camera's intrinsic parameters is because the actual camera projection process and the

pinhole model are not completely corresponding, and the equivalent camera optical center points at different distances are different [13]. Barrel distortion usually occurs at short focal lengths, and pincushion distortion usually occurs at long focal lengths [33]. To evaluate the camera's intrinsic calibration instability, We designed the camera intrinsic calibration consistency experiment. We used the camera to collect 6 uniformly distributed checkerboard image groups, and each group contained 100 frames. Then, we randomly selected 25 images from each group for the camera's intrinsic calibration, performed 100 times per group. We obtained the residual vector whose statistical information (e.g. mean, variance) reveals the camera's intrinsic calibration volatility. The results are shown in Fig. 7.

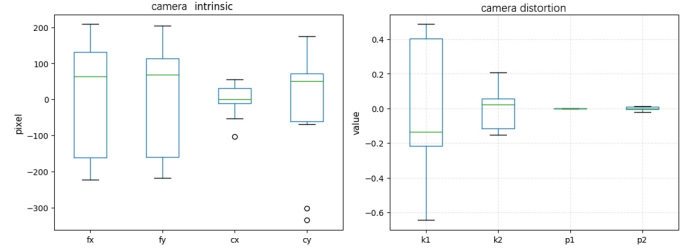


Fig. 7: Camera's intrinsic parameter calibration comparison.

2) *Ablation experiment*: We designed an ablation experiment to evaluate our method better to split our one-stage approach into a two-stage process. Then, we respectively compared the 3D-2D reprojection error of the circles center and checkerboard corners on the calibration board. We conducted six sets of experiments, each was calibrated with one-stage and two-stage respectively and compared the reprojection error of their checkerboard and the circles center. As shown in Table I, our method has a smaller reprojection error of the circles center than the two-stage calibration.

TABLE I: Average Reprojection Error for One-stage and Two-stage Calibration

| | Checkboard Corners | Circles Center |
|-----------|--------------------|----------------|
| One-stage | 0.757 pixel | 1.104 pixel |
| Two-stage | 0.546 pixel | 5.428 pixel |

3) *Qualitative Results*: To better visualize the performance of our method, the point cloud is projected to the image plane using the intrinsic and extrinsic parameters calibrated by our method. Results are shown in Fig. 8. As shown, using the calibration parameters extracted by the proposed approach enables a perfect alignment between both data modalities. Fig. 9 shows the effect of circles center reprojection on the calibration board.

4) *Comparison Experiments*: We compared our methods with [23] and [30], which both use checkerboard as a calibration target. The first one method [23] estimates the extrinsic by minimizing the distance from LiDAR points to the checkerboard plane estimated from the image. The second method [30] estimates the extrinsic by ArUco markers

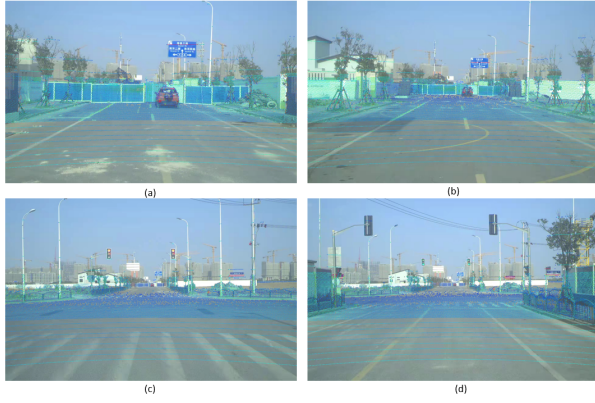


Fig. 8: Point cloud projections in four different scenarios, projection points color is represented by the LiDAR intensity.

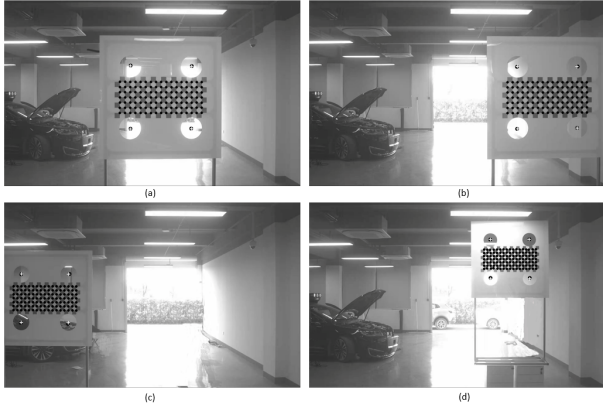


Fig. 9: Realistic Experiment: Reprojection of the circles center on the calibration board. The black circle is the LiDAR projection point, and the white cross is the calculated image point.

and circles center registration on the calibration board. We first spent a lot of effort calibrating the camera's intrinsic parameter. As shown in Fig. 10, the A and B boxed in the image show that the distortion effect is good. However, due to the small error of the camera focal length and optical center, the parameters calibrated by the method [23] and [30] still cannot align the point cloud and the image in some places. For this case, our method can adjust the intrinsic parameters so that the point cloud and the image are perfectly aligned.

B. Simulated Experiment

We also conducted experiments with our method in the simulation environment. We generated 3 calibration data groups in the Carla engine [32], and each group consists of 33 frames. We quantitatively compared the mean of LiDAR-camera extrinsic calibration with the ground truth in Table II. Fig. 10 also shows the effect of circles center reprojection on the calibration board. The result shows the proposed method can achieve accuracy and robustness performance.

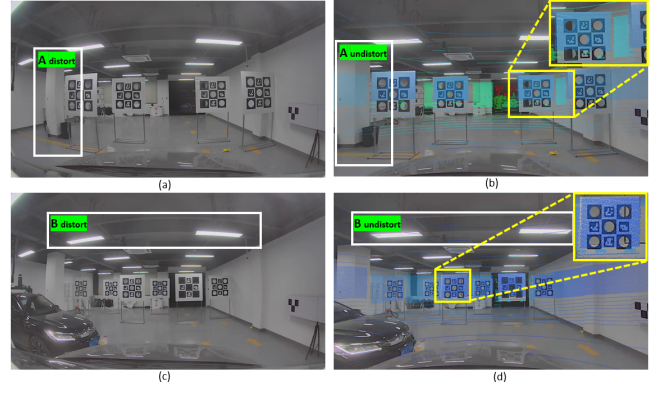


Fig. 10: LiDAR-camera extrinsic calibration by the method [30].

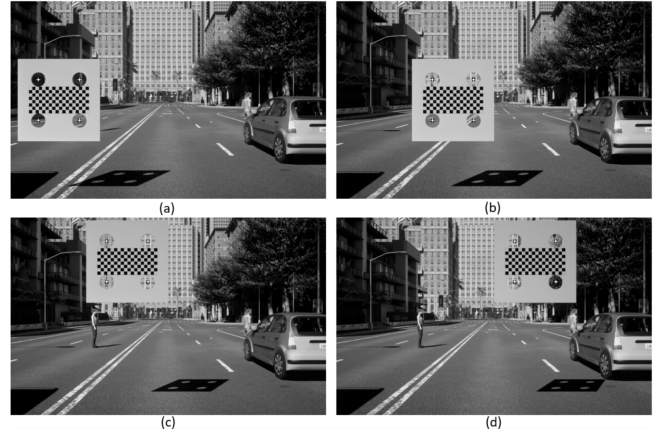


Fig. 11: Simulated Experiment: Reprojection of the circles center on the calibration board. The black circle is the LiDAR projection point, and the white cross is the calculated image point.

V. CONCLUSIONS

This paper proposes a novel target-based calibration method, joint camera intrinsic and LiDAR-Camera extrinsic calibration. Qualitative and quantitative results demonstrate the performance and effectiveness of our method. The related codes and data have been open-sourced to benefit the community.

In the real environment, due to the sparsity of the point cloud, the extraction accuracy of the circle center may decrease. In the future, we look forward to using the multi-frame data of vehicle motion to increase the density of the point cloud, thereby improving the extraction accuracy of the circle center to improve the calibration performance further.

TABLE II: Translation and Rotation Quantitative Evaluation.

| | $t_x(m)$ | $t_y(m)$ | $t_z(m)$ | $roll(^{\circ})$ | $pitch(^{\circ})$ | $yaw(^{\circ})$ |
|-----|----------|----------|----------|------------------|-------------------|-----------------|
| GT | 0 | 0.595 | 2.5 | -90 | 0 | 90 |
| Our | -0.001 | 0.5912 | 2.5079 | -90.002 | 0.011 | 90.004 |

REFERENCES

- [1] C. Guindel, J. Beltrán, D. Martín, and F. García, "Automatic extrinsic calibration for lidar-stereo vehicle sensor setups," in *2017 IEEE 20th International Conference on Intelligent Transportation Systems (ITSC)*, 2017, pp. 1–6.
- [2] H. Cai, W. Pang, X. Chen, Y. Wang, and H. Liang, "A novel calibration board and experiments for 3d lidar and camera calibration," *Sensors*, vol. 20, no. 4, 2020. [Online]. Available: <https://www.mdpi.com/1424-8220/20/4/1130>
- [3] P. An, T. Ma, K. Yu, B. Fang, J. Zhang, W. Fu, and J. Ma, "Geometric calibration for lidar-camera system fusing 3d-2d and 3d-3d point correspondences," *Opt. Express*, vol. 28, no. 2, pp. 2122–2141, Jan 2020. [Online]. Available: <http://opg.optica.org/oe/abstract.cfm?URI=oe-28-2-2122>
- [4] W. Wang, K. Sakurada, and N. Kawaguchi, "Reflectance intensity assisted automatic and accurate extrinsic calibration of 3d lidar and panoramic camera using a printed chessboard," *Remote Sensing*, vol. 9, no. 8, 2017. [Online]. Available: <https://www.mdpi.com/2072-4292/9/8/851>
- [5] J. Liu, Z. Yang, H. Huo, and T. Fang, "Camera calibration method with checkerboard pattern under complicated illumination," *Journal of Electronic Imaging*, vol. 27, no. 4, pp. 1 – 11, 2018. [Online]. Available: <https://doi.org/10.1117/1.JEI.27.4.043038>
- [6] B. Chen, Y. Liu, and C. Xiong, "Automatic checkerboard detection for robust camera calibration," in *2021 IEEE International Conference on Multimedia and Expo (ICME)*, 2021, pp. 1–6.
- [7] J. Kümmerle, T. Kühner, and M. Lauer, "Automatic calibration of multiple cameras and depth sensors with a spherical target," in *2018 IEEE/RSJ International Conference on Intelligent Robots and Systems (IROS)*, 2018, pp. 1–8.
- [8] S. Sels, B. Ribbens, S. Vanlanduit, and R. Penne, "Camera calibration using gray code," *Sensors*, vol. 19, no. 2, 2019. [Online]. Available: <https://www.mdpi.com/1424-8220/19/2/246>
- [9] J. Zhang, J. Zhu, H. Deng, Z. Chai, M. Ma, and X. Zhong, "Multi-camera calibration method based on a multi-plane stereo target," *Appl. Opt.*, vol. 58, no. 34, pp. 9353–9359, Dec 2019. [Online]. Available: <http://opg.optica.org/ao/abstract.cfm?URI=ao-58-34-9353>
- [10] Y. Zhu, C. Li, and Y. Zhang, "Online camera-lidar calibration with sensor semantic information," in *2020 IEEE International Conference on Robotics and Automation (ICRA)*, 2020, pp. 4970–4976.
- [11] Z. Zhang, "A flexible new technique for camera calibration," *IEEE Transactions on Pattern Analysis and Machine Intelligence*, vol. 22, no. 11, pp. 1330–1334, 2000.
- [12] R. S. Sturm P. and L. S., "Imaging beyond the pinhole camera," in *On Calibration, Structure from Motion and Multi-View Geometry for Generic Camera Models*, 2006, pp. 1–8.
- [13] R. Juárez-Salazar, J. Zheng, and V. H. Díaz-Ramírez, "Distorted pinhole camera modeling and calibration," *Applied Optics*, vol. 59, no. 36, pp. 11 310–11 318, 2020.
- [14] A. de la Escalera and J. Armingol, "Automatic chessboard detection for intrinsic and extrinsic camera parameter calibration," *Sensors (Basel, Switzerland)*, vol. 10, pp. 2027–44, 03 2010.
- [15] O. Bogdan, V. Eckstein, F. Rameau, and J.-C. Bazin, "Deepcalib: A deep learning approach for automatic intrinsic calibration of wide field-of-view cameras," in *Proceedings of the 15th ACM SIGGRAPH European Conference on Visual Media Production*, ser. CVMP '18. New York, NY, USA: Association for Computing Machinery, 2018. [Online]. Available: <https://doi.org/10.1145/3278471.3278479>
- [16] B. Jin, H. Lei, and W. Geng, "Accurate intrinsic calibration of depth camera with cuboids," in *Computer Vision – ECCV 2014*, D. Fleet, T. Pajdla, B. Schiele, and T. Tuytelaars, Eds. Cham: Springer International Publishing, 2014, pp. 788–803.
- [17] G. H. An, S. Lee, M.-W. Seo, K. Yun, W.-S. Cheong, and S.-J. Kang, "Charuco board-based omnidirectional camera calibration method," *Electronics*, vol. 7, no. 12, 2018. [Online]. Available: <https://www.mdpi.com/2079-9292/7/12/421>
- [18] M. Lopez, R. Mari, P. Gargallo, Y. Kuang, J. Gonzalez-Jimenez, and G. Haro, "Deep single image camera calibration with radial distortion," in *Proceedings of the IEEE/CVF Conference on Computer Vision and Pattern Recognition (CVPR)*, June 2019.
- [19] B. Khaleghi, A. Khamis, F. O. Karray, and S. N. Razavi, "Multisensor data fusion: A review of the state-of-the-art," *Inf. Fusion*, vol. 14, no. 1, p. 28–44, Jan. 2013. [Online]. Available: <https://doi.org/10.1016/j.inffus.2011.08.001>
- [20] Q. Zhang and R. Pless, "Extrinsic calibration of a camera and laser range finder (improves camera calibration)," in *2004 IEEE/RSJ International Conference on Intelligent Robots and Systems (IROS) (IEEE Cat. No.04CH37566)*, vol. 3, 2004, pp. 2301–2306 vol.3.
- [21] A. Geiger, F. Moosmann, Ö. Car, and B. Schuster, "Automatic camera and range sensor calibration using a single shot," in *2012 IEEE International Conference on Robotics and Automation*, 2012, pp. 3936–3943.
- [22] J.-K. Huang and J. W. Grizzle, "Improvements to target-based 3d lidar to camera calibration," *IEEE Access*, vol. 8, pp. 134 101–134 110, 2020.
- [23] L. Zhou, Z. Li, and M. Kaess, "Automatic extrinsic calibration of a camera and a 3d lidar using line and plane correspondences," in *2018 IEEE/RSJ International Conference on Intelligent Robots and Systems (IROS)*, 2018, pp. 5562–5569.
- [24] J. Levinson and S. Thrun, "Automatic online calibration of cameras and lasers," in *Robotics: Science and Systems*, vol. 2, 2013, p. 7.
- [25] T. Ma, Z. Liu, G. Yan, and Y. Li, "Crlf: Automatic calibration and refinement based on line feature for lidar and camera in road scenes," 2021.
- [26] G. Pandey, J. R. McBride, S. Savarese, and R. M. Eustice, "Automatic extrinsic calibration of vision and lidar by maximizing mutual information," *Journal of Field Robotics*, vol. 32, no. 5, pp. 696–722, 2015.
- [27] Z. Taylor and J. I. Nieto, "Automatic calibration of lidar and camera images using normalized mutual information," 2012.
- [28] M. Velas, M. Spanel, Z. Materna, and A. Herout, "Calibration of rgb camera with velodyne lidar," 2014.
- [29] G. Bradski, "The OpenCV Library," *Dr. Dobbs's Journal of Software Tools*, 2000.
- [30] J. Beltrán, C. Guindel, and F. García, "Automatic extrinsic calibration method for lidar and camera sensor setups," *arXiv preprint arXiv:2101.04431*, 2021.
- [31] S. Agarwal, K. Mierle, and Others, "Ceres solver," <http://ceres-solver.org>.
- [32] A. Dosovitskiy, G. Ros, F. Codevilla, A. Lopez, and V. Koltun, "CARLA: An open urban driving simulator," in *Proceedings of the 1st Annual Conference on Robot Learning*, 2017, pp. 1–16.
- [33] F. Bukhari and M. N. Dailey, "Automatic radial distortion estimation from a single image," *Journal of mathematical imaging and vision*, vol. 45, no. 1, pp. 31–45, 2013.